International Journal of General Medicine

Dovepress
open access to scientific and medical research

Open Access Full Text Article

ORIGINAL RESEARCH

CT Features of Stage IA Invasive Mucinous Adenocarcinoma of the Lung and Establishment of a Prediction Model

Xiuming Zhang[1,*], Wei Qiao[1,*], Zheng Kang[1], Chunhan Pan[1], Yan Chen[2], Kang Li[1], Wenrong Shen[1], Lei Zhang[1]

[1]Department of Radiology, Jiangsu Cancer Hospital & Jiangsu Institute of Cancer Research & The Affiliated Cancer Hospital of Nanjing Medical University, Nanjing, Jiangsu, People's Republic of China; [2]Department of Pathology, Jiangsu Cancer Hospital & Jiangsu Institute of Cancer Research & The Affiliated Cancer Hospital of Nanjing Medical University, Nanjing, Jiangsu, People's Republic of China

*These authors contributed equally to this work

Correspondence: Lei Zhang; Wenrong Shen, Email motozl163@163.com; jszlyyct@sohu.com

Objective: To investigate computed tomography (CT) features of stage IA invasive mucinous adenocarcinoma (IMA) of the lung and establish a predictive model.

Methods: Fifty-three lesions from 53 cases of stage IA IMA between January 2017 and December 2019 were examined, while 141 lesions from 141 cases of invasive non-mucinous lung adenocarcinoma (INMA) served as control cases. Univariate analysis was performed to compare differences in demographics and CT features between the two groups, and multivariate logistic regression analysis was performed to determine primary influencing factors of solitary nodular IMA. A risk score prediction model was established based on the regression coefficients of these factors, and receiver operating characteristic (ROC) curve analysis was performed to evaluate the predictive performance of the model.

Results: Univariate analysis showed that age, nodule type, maximum nodule diameter, tumor lung interface, lobulation, spiculation, air bronchogram or vacuolar signs, and abnormal vascular changes differed significantly between the two groups ($p < 0.05$). Compared to INMA, spiculation of IMA was relatively longer and softer. Multivariate logistic regression analysis showed that nodule type, indistinct tumor lung interface, air bronchogram or vacuolar signs, and abnormal vascular changes were the primary influencing factors. A prediction model based on the regression coefficients of these factors was established. ROC curve analysis indicated that the area under the curve was 0.882 ($p < 0.05$).

Conclusion: Compared to INMA, solitary peripheral stage IA nodular IMA were more common in older patients; they more frequently had indistinct tumor lung interface and air bronchogram or vacuolar signs on CT; spiculation was relatively longer and softer; our risk score prediction model based on nodule type, tumor lung interface, air bronchogram or vacuolar signs, and abnormal vascular changes was established with good predictive efficacy for solitary nodular IMA.

Keywords: invasive mucinous adenocarcinoma of the lung, influencing factors, risk score modeling

Background

In 2015, the World Health Organization Classification of Lung Tumors was updated their classification criteria for lung cancers. According to these criteria, adenocarcinomas were divided into non-mucinous adenocarcinomas and adenocarcinoma variants. In addition, the term "invasive mucinous lung adenocarcinoma (IMA)" was introduced to replace adenocarcinomas previously classified as mucinous bronchioloalveolar adenocarcinomas.[1] According to the report, IMA accounts for 0.2% of all primary lung cancers and 2–10% of all lung adenocarcinomas,[2] and is thus considered a relatively rare histological subtype. Due to its low incidence, the clinical and pathological characteristics and prognosis of IMA are unclear and debatable. Some studies have suggested that the overall prognosis is worse for IMA than for non-mucinous adenocarcinoma of the lung,[3,4] with airway dissemination occurring at early stages;[5,6] hence, early detection

Received: 2 April 2022
Accepted: 23 May 2022
Published: 4 June 2022

and diagnosis are particularly important for local control. We aim to diagnose or predict solitary nodular IMA at early stages by analyzing demographic and computed tomography (CT) characteristics of patients with solitary nodular IMA and to establish a prediction model in order to help clinicians design optimal treatment strategies.

Objective

This study aimed to investigate CT features of solitary stage IA nodular invasive mucinous adenocarcinoma (IMA) of the lung and establish a predictive model.

Materials and Methods

General Data

A total of 3470 cases with lung lesions were confirmed by surgical pathology as lung adenocarcinoma at Jiangsu cancer hospital from January 2017 to December 2019 were examined, including 159 cases of mucinous adenocarcinoma. Patients were excluded from the study cohort if any of the following conditions were met: 1. Other concomitant tumor components; 2. Lung adenocarcinoma of tumor node metastasis (TNM) stage IB or above; 3. Multiple nodules; 4. pneumonia-type lung adenocarcinoma. In addition, 141 cases of patients with stage IA non-mucinous adenocarcinoma admitted to our hospital during the same period were randomly selected as the control group (Figure 1).

The experimental data collection was approved by the Ethics Committee of Jiangsu Cancer Hospital. The study obtained the informed consent from the study participants prior. It was not considered to impose an additional burden on patients, cause injury to patients or affect their treatment, and did not violate patients' privacy. We confirm that the study complies with the Declaration of Helsinki.

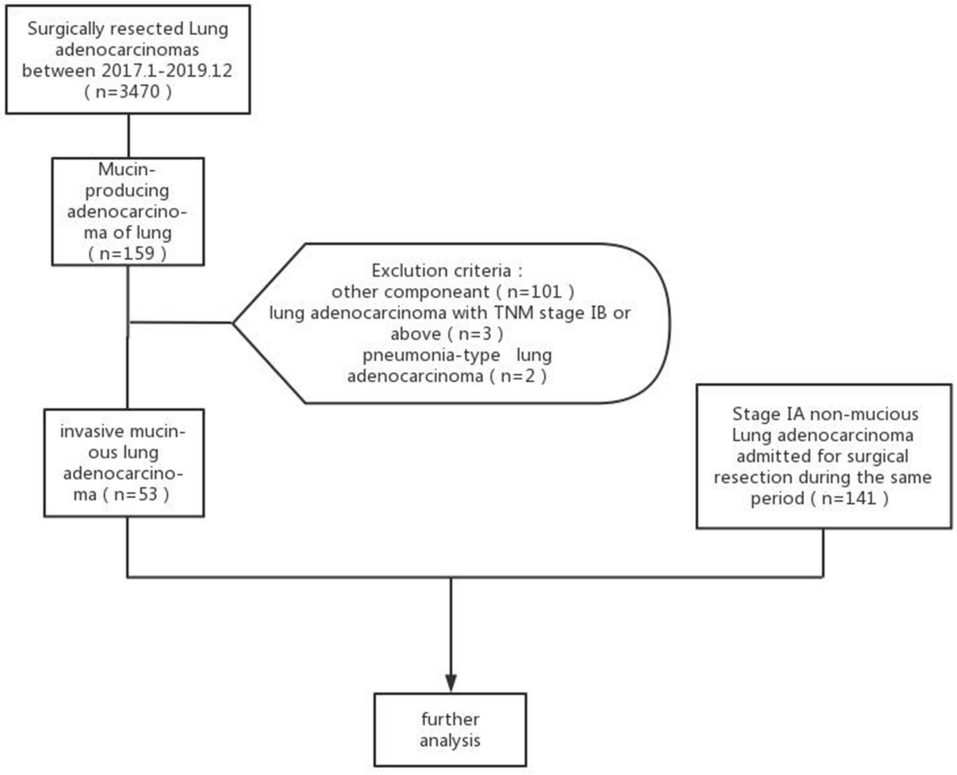

Figure 1 Flow diagram shows patient selection and exclusion criteria.

Examinations

The Discover 750HD spectral CT and LightSpeed VCT (GE Healthcare, USA) instruments were used for examinations. Patients were placed in the supine position. Scans ranged from the thoracic inlet to the base of the diaphragm. Scan slice thickness was 0.625 mm * 64. For image reconstruction, slice spacing was 1.25 mm and 5 mm, slice thickness was 1.25 mm and 5 mm, tube voltage was 80–120 kV, and tube current was 200–280 mA. Out of all patients, 90.72% (176/194) underwent enhanced CT scanning, patients were rapidly injected with ioversol by high-pressure syringe at a dose of 1.5 ml/kg, and scanning started after a delay of approximately 30 seconds.

Image Analysis

CT observational indicators included maximum nodule diameter, nodule morphology (spherical, spheroid, or clearly irregular), tumor lung interface (distinct, indistinct), spiculation, lobulation, internal features (air bronchogram or vacuolar signs), abnormal vascular changes (broncho vascular bundle sign, CT tumor microvascular sign), and pleural retraction. According to consolidation tumor ratio (CTR), all lesions were divided into two types: type I: solid nodules (ST) and part solid nodule (PSN) with CTR ≥0.5, Type II: pure ground glass nodules (PGGN) and PSN with CTR< 0.5. Comprehensive image analysis was performed by two physicians with over 10 years of experience in chest imaging diagnosis and consensus was reached.

Statistics

SPSS 26 was used for data analysis. The K–S test was performed to determine whether continuous variables conformed to normal distribution. The unpaired *t*-test was used for variables conforming to normal distribution, and analysis of variance and the Mann–Whitney *U*-test were used for variables not conforming to normal distribution. The chi-square test, chi-square test with correction for continuity, or Fisher's exact test were used to compare differences in CT characteristics between groups. Factors with significant differences in univariate analysis were entered into multivariate logistic regression analysis to obtain the primary influencing factors and their regression coefficients. The risk score model was used to calculate the total risk score of each primary influencing factor. Finally, the receiver operating characteristic (ROC) curve was plotted to evaluate the predictive power of the model. Differences with $p < 0.05$ were considered statistically significant.

Results

Univariate Analysis

Univariate analysis revealed a significant difference in age between the two groups, with the IMA group having higher age ($p < 0.05$). There was a statistically significant difference in nodule type between the two groups. Type I were more common in IMA (83.02%, 44/53 patients), and Type II were more common in INMA (65.25%, 92/141 patients). Regarding CT features, there were statistically significant differences in maximum nodule diameter, tumor lung interface, lobulation, spiculation, air bronchogram or vacuolar signs, and abnormal vascular changes between the two groups ($p < 0.05$). In the IMA group, maximum nodule diameter was larger, the tumor lung interface was more often indistinct (24.53% vs 2.13%, $p < 0.05$) (Figure 2A–C, white arrows), the vacuolar sign (Figure 2A–C, black arrows) or air bronchogram sign (Figure 3A, black arrows) was present more frequently (64.15% vs 24.11%, $p < 0.05$), and the frequency of lobulation (60.38% vs 43.26%, $p < 0.05$) and spiculation (58.49% vs 38.3%, $p < 0.05$) was relatively higher. In addition, spiculation was longer and softer in the IMA group (Figure 3A–C white arrows), and abnormal vascular changes were less common (77.36% vs 91.49%, $p < 0.05$). There were no significant differences in nodule morphology or pleural retraction between the two groups ($p > 0.05$), but irregular morphology (Figure 4A–C) was more common in the IMA group than in the INMA group (15.09% vs 9.92%, $p > 0.05$) (Table 1). All patients had pathological results (Figures 2D,3D and 4D).

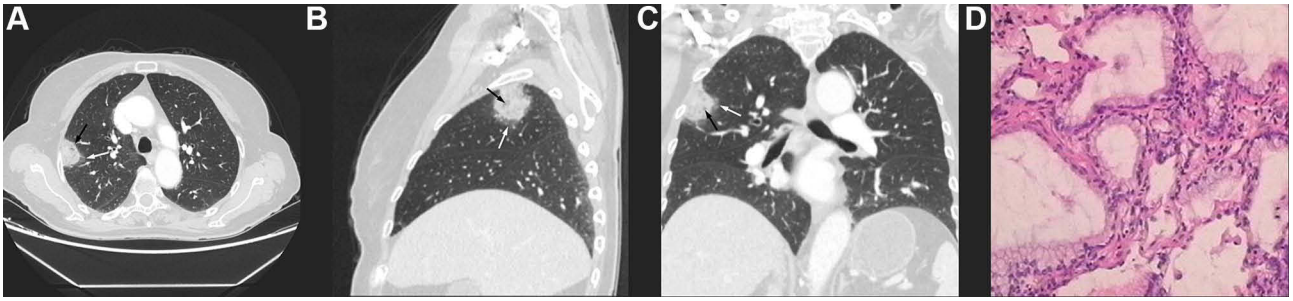

Figure 2 (**A**–**C**) CT of a 73-year-old female indicated a subpleural solid nodule lateral of the apex of the right upper lung. The tumor lung interface was indistinct (white arrow), the internal structure was diffuse, and multiple small "vacuoles" were observed (black arrows). (**D**) Pathology (HE stain 400 X) indicated invasive mucinous lung adenocarcinoma (IMA).

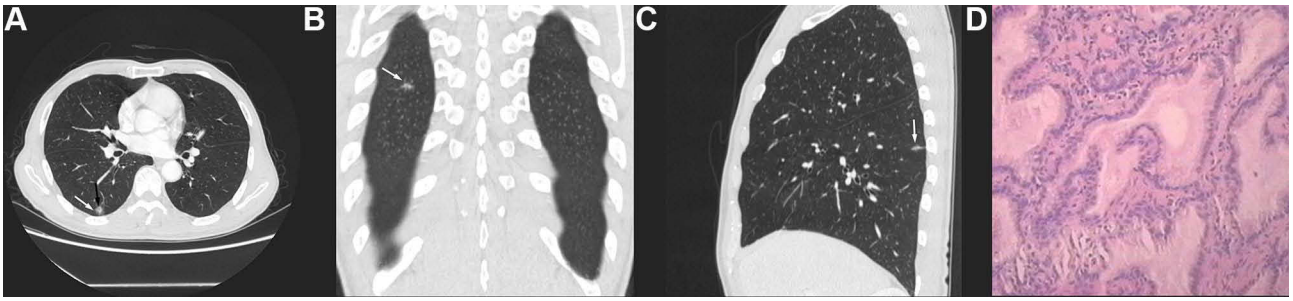

Figure 3 (**A**–**C**) CT of a 67-year-old male indicated a part-solid nodule in the dorsal segment of the right lower lung with irregular morphology and "rambutan"-like, long and soft spiculation (white arrows) at the margins and air bronchogram sign in the center (black arrow). (**D**) Pathology (HE stain 400 X) indicated IMA.

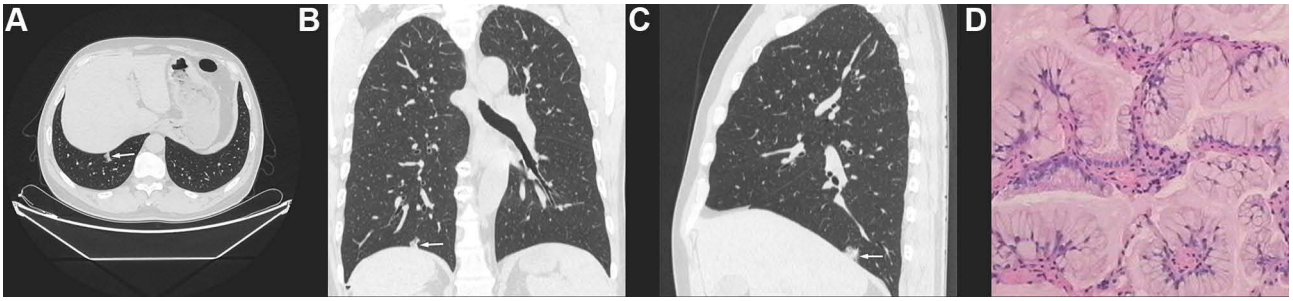

Figure 4 (**A**–**C**) CT of a 59-year-old male indicated a part-solid nodule in the posterior basal segment of the right lower lung, with predominant consolidation components, clearly irregular morphology, and relatively straight margins. (**D**) Pathology (HE stain 400 X) indicated IMA.

Multivariate Logistic Regression Analysis

Multivariate logistic regression analysis showed that nodule type (OR = 23.335; $p < 0.05$), indistinct tumor lung interface (OR = 15.974; $p < 0.05$), air bronchogram or vacuolar signs (OR = 9.98; $p < 0.05$), and abnormal vascular changes (OR = 0.107; $p < 0.05$) were the primary influencing factors (Table 2).

Establish and Evaluate the Risk Score Model

Establishment of the prediction model: The risk score model was expressed as risk score all (RA) = 3.150 * nodule type + 2.771 * tumor lung interface + 2.301 * air bronchogram or vacuolar sign - 2.231 * abnormal vascular changes - 3.066.

Evaluation of predictive power: The calculated total risk score of the 194 cases was plotted as a ROC curve (Figure 5). The area under the ROC curve (blue) of the total risk score was 0.882 ($p < 0.05$). At a cutoff point of 0.593, the model had a sensitivity of 69.2%, a specificity of 90.1%, and a 95% confidence interval of (0.833, 0.931).

Table 1 Univariate Analysis of Differences in Nodule Type, Demographic Differences and CT Features Between the Invasive Mucinous Adenocarcinoma and Invasive Non-Mucinous Lung Adenocarcinoma Groups

		IMA (N=53)	INMA (N=141)	Statistic	*P*
Sex				1.47	0.225
M		25 (47.17)	53 (37.59)		
F		28 (52.83)	88 (62.41)		
Age (years)		70.89±14.50	58.52±9.57	5.76	**0***
Nodule type					**0[a]**
I		44 (83.02)	92 (65.25)		
II		9(16.98)	49 (34.75)		
Size (cm)		1.80±0.73	1.44±0.59		**0.002****
Morphology	Clearly irregular	8 (15.09)	14 (9.92)	1.022	0.312
	Spherical or spheroid	45 (84.91)	127 (90.08)		
Tumor lung interface	Indistinct	13 (24.53)	3 (2.13)	22.669	**0**
	Distinct	40 (75.47)	138 (97.87)		
Lobulation	Yes	32 (60.38)	61 (43.26)	4.521	**0.033**
	No	21 (39.62)	80 (56.74)		
Spiculation	Yes	31 (58.49)	54 (38.3)	6.38	**0.012**
	No	22 (41.51)	87 (61.7)		
Air bronchogram or vacuolar sign	Yes	34 (64.15)	34 (24.11)	27.124	**0**
	No	19 (35.85)	107 (75.89)		
Abnormal vascular changes	Yes	41 (77.36)	129 (91.49)	7.095	**0.008**
	No	12 (22.64)	12 (8.51)		
Pleural retraction	Yes	33 (62.26)	79 (56.03)	0.614	0.433
	No	20 (33.74)	62 (43.97)		

Notes: *Normal distribution (unpaired *t*-test) with statistical significance (*P*<0.05); **non-normal distribution (Mann–Whitney *U*-test) with statistical significance (*P*<0.05); [a]fisher exact test. Bold values referred to significant variables (p < 0.05) in univariate analysis.

Table 2 Multivariate Logistic Regression Analysis of Independent Factors Influencing Invasive Mucinous Adenocarcinoma

Variable	B	*P*	Odds Ratio (95% Confidence Intervall)
Age	0.649	0.173	1.914 (0.753,4.866)
Nodule type	3.15	**0**	23.335 (5.665,96.118)
Maximum nodule diameter	0.101	0.849	1.106 (0.391,3.126)
Tumor lung interface	2.771	**0.003**	15.974 (2.595,98.335)
Lobulation	−1.111	0.085	0.329 (0.093,1.167)
Spiculation	0.568	0.309	1.765 (0.59,5.28)
Air bronchogram or vacuolar signs	2.301	**0**	9.98 (3.846,25.892)
Abnormal vascular changes	−2.231	**0.005**	0.107 (0.023,0.502)
Constant	−3.066	0.003	0.047

Note: Bold values referred to significant variables (p < 0.05) in multivariate logistic regression analysis.

Discussion

In 2015, the WHO identified IMA of the lung as a variant of lung adenocarcinoma with low incidence, composed of goblet cells or tall columnar epithelium, abundant intracytoplasmic mucin, and uniform basal nuclei on pathology.[7,8] The incidence of epidermal growth factor receptor (EGFR) mutations is lower in IMA than in INMA, whereas the incidence of KRAS mutations is higher in IMA than in INMA.[9] IMA can spread to short distances at early stages and to more distant lung parenchyma in advanced stages. Previous studies on IMA prognosis have been controversial, with some studies showing that prognosis is worse for IMA than for INMA. Due to the low mutation rate of EGFR,

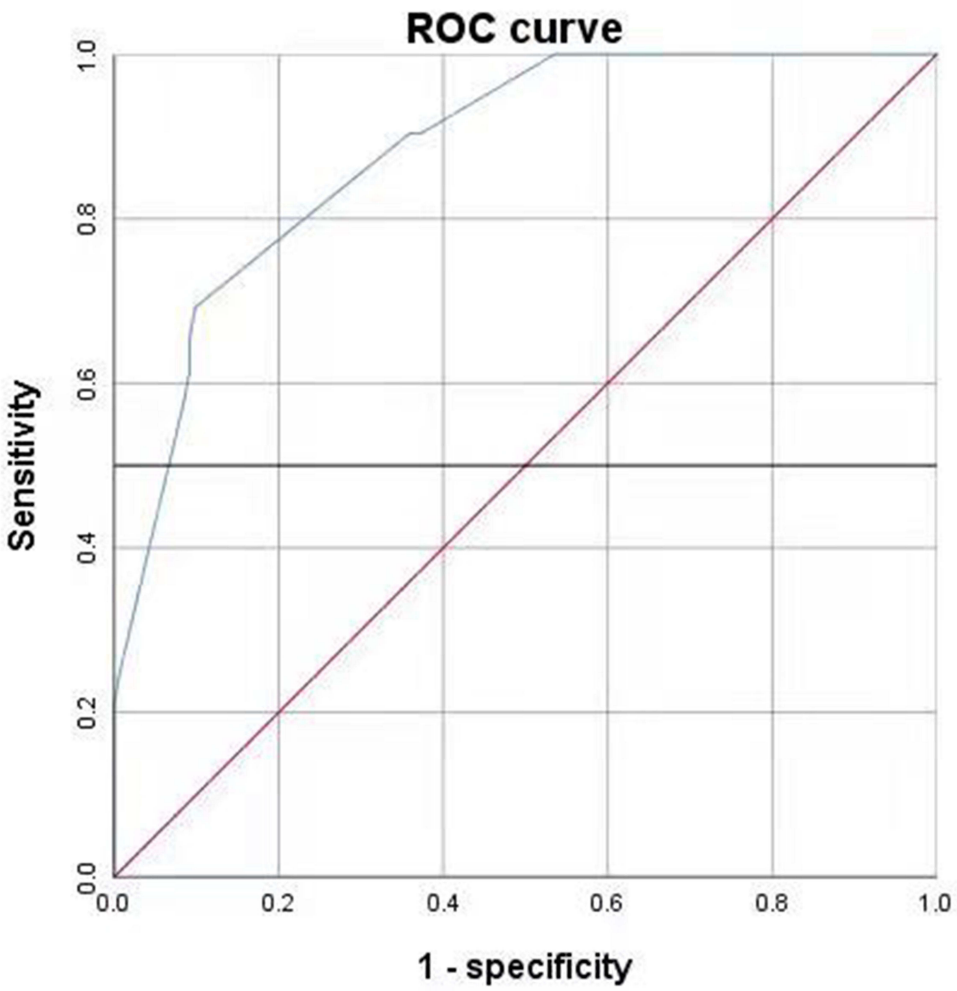

Figure 5 The ROC curve used to evaluate the risk score prediction model.

chemotherapeutic agents targeting EGFR are unlikely to be effective. Some researchers have found that chemotherapy (non-TKI, platinum-based) does not improve the overall survival (OS) of most patients with advanced IMA.[10] Surgical resection is still recommended for patients with clinical stage I IMA.[11] In addition, due to the high rate of airway dissemination (50–70%), these patients develop resistance to systemic intravenous chemotherapy; some researchers have suggested that respiratory therapy maybe effective.[5] B7-H4 is expressed in IMA and is, therefore, considered as a target for immunotherapy.[12] Because of the many differences between IMA and INMA with respect to clinical, pathological, immunological, and genetic factors involved, and treatment methods, it is particularly important to identify and screen for IMA through radiological studies in order to design optimal treatment strategies.

The majority of studies have classified IMA into pneumonia-type and solitary nodular types based on CT findings. For pneumonia-type IMA, mixed consolidation, air bronchogram or vacuolar signs, and CT vascular opacities are characteristic CT findings, which are combined with a large amount of mucin and tumor infiltration on pathology.[5,13] The clinical and pathological features and CT signs of the solitary nodular type of IMA have rarely been reported. Miyata et al[14] reported a number of cases with surgically resected mucinous AIS/MIA and found that they were characterized by solid and part-solid nodules and ground-glass opacities with lobular-bounded margins or marginally vaguely outlined ground-glass opacities, reflecting histological features associated with mucin in air-containing spaces and macrophage infiltration and invasion of tumor cells, with a few cases of pleural indentation, spiculation, and abnormal vascular changes. It is unclear whether these characteristics are maintained in IMA.

Univariate analysis showed statistically significant differences in age, nodule type, maximum nodule diameter, tumor lung interface, lobulation, spiculation, air bronchogram or vacuolar signs, and abnormal vascular changes between the solitary nodular IMA and INMA groups ($p < 0.05$), but no significant differences in sex, nodule morphology, pleural retraction, and relative contrast-enhanced CT values ($p > 0.05$). Multivariate logistic regression analysis showed that nodule type (OR = 23.335; $p < 0.05$), indistinct tumor lung interface (OR = 15.974; $p < 0.05$), air bronchogram or vacuolar signs (OR = 9.98; $p < 0.05$), and abnormal vascular changes (OR = 0.107; $p < 0.05$) were the primary influencing factors.

With respect to nodule types, we found that solid nodules and nodules with CTR greater than or equal to 0.5 were more common in IMA (83.02%, 44/53), whereas nodules with PGGN and CTR less than 0.5 were more common in INMA (65.25%, 92/141), consistent with previous studies.[14]

The tumor lung interface was indistinct in 24.53% (13/53) of IMA cases, whereas the incidence of this finding was only 2.3% (3/141) among INMA cases, indicating a statistically significant, consistent with previous studies.[13,14] Pathologically, the indistinct tumor lung interface is due to mucus extravasation from the margin of the nodule and migration of macrophages along the alveolar walls and pores to regions far from the nodule, resulting in an indistinct and irregular interface. In contrast, ground-glass opacities in INMA are relatively distinct and regular, and imaging finding show that the normal alveolar epithelium is partially replaced by tumor cells and the alveolar cavity is not completely filled.[15] Although the incidence of this finding is low, it is indeed one of the major CT features that distinguishes IMA from other types of stage IA lung cancer.

The incidence of the air bronchogram or vacuolar signs in IMA (64.15%, 34/53) was statistically significantly higher than in INMA (24.11%, 34/141). Solitary nodular IMA has been reported to be prone to cavitary lung lesions (air bronchogram or vacuolar signs).[16,17] The pathological causes of these signs include: 1. Expulsion of mucus from mucus pools through the attached bronchi. 2. Invasive tumor growth along the terminal airway and secretion of mucus, which inhibits the respiratory valve-like function of the airway. Air enters easily but cannot exit, leading to air cavities formed by the rupture of alveoli after overinflation. 3. Formation of tumor-free areas that are composed of normal alveolar cavities. 4. Degradation of hydrolase within tumors leading to destruction of air cavities formed by normal alveolar interstitial elastic fibers.

In addition, univariate analysis revealed significant differences in lobulation, spiculation, and abnormal vascular changes between the two groups. These reliable CT features that characterize solitary nodule or mass lung cancer are also useful morphological features for IMA diagnosis.[18] However, the present study found that the appearance of the spiculation sign differed between IMA and INMA, with the sign being longer and softer in the former, similar to a rambutan fruit. Possible causes include 1. Large amounts of mucin in the cytoplasm of IMA tumor cells. 2. Abundant presence of extracellular mucus in tumor cells when infiltrating along the alveolar interstitium. 3. Tumor neovascularization.

In addition to the indistinct tumor lung interface, irregular nodule morphology is also a major cause of misdiagnosis of stage IA lung adenocarcinoma,[19,20] with one study reporting a misdiagnosis rate of early IMA of 35%.[14] In addition, although the difference was not statistically significant, in our cohort the morphology was more irregular in IMA than in INMA patients (15.09% vs 9.92%). For nodules with indistinct margins and irregular morphology, CT re-examination after short-term anti-inflammatory treatment is necessary, as shown in our previously published recommendations on examination techniques and specifications for radiological reading of stage IA lung adenocarcinoma.

Taken together, we conclude that solitary nodular IMA maintains the CT features of mucinous AIS/MIA, such as indistinct tumor lung interface and air bronchogram or vacuolar signs. However, due to the increased presence of infiltrating components, IMA differs from AIS and MIA, because it also exhibits CT signs of solitary nodule or mass-type stage IA lung adenocarcinoma such as lobulation, spiculation, and abnormal vascular changes; the differences were significant compared to INMA ($p < 0.05$).

The ROC curve used to evaluate the risk score prediction model was 0.882 ($p < 0.05$), indicating that the model has good predictive power and has practical application in patients.

In conclusion, compared to INMA, solitary peripheral stage IA nodular IMA were more common in older patients; they were more frequently had indistinct tumor lung interface and air bronchogram or vacuolar signs on CT; spiculation

was relatively longer and softer; Our risk score prediction model based on tumor lung interface, air bronchogram or vacuolar signs, spiculation, and abnormal vascular changes was established with good predictive efficacy for IMA.

Author Contributions

All authors made a significant contribution to the work reported, whether that is in the conception, study design, execution, acquisition of data, analysis and interpretation, or in all these areas; took part in drafting, revising or critically reviewing the article; gave final approval of the version to be published; have agreed on the journal to which the article has been submitted; and agree to be accountable for all aspects of the work.

Funding

This work was supported by the Roentgen special fund for image research of Jiangsu Medical Association (SYH-32011500008 2021003) and the Jiangsu Cancer Hospital Young Talents Plan (Jiangsu China).

Disclosure

The authors declare no conflicts of interest in this work.

References

1. Travis WD, Brambilla E, Nicholson AG, et al. The 2015 World Health Organization classification of lung tumors: impact of genetic, clinical and radiologic advances since the 2004 classification. *J Thorac Oncol*. 2015;10(9):1243–1260. doi:10.1097/JTO.0000000000000630
2. Moon SW, Si YC, Mi HM, et al. Effect of invasive mucinous adenocarcinoma on lung cancer-specific survival after surgical resection: a population-based study. *J Thorac Dis*. 2018;10(6):3595–3608. doi:10.21037/jtd.2018.06.09
3. Dacic S. Pros: the present classification of mucinous adenocarcinomas of the lung. *Transl Lung Cancer Res*. 2017;6(2):230. doi:10.21037/tlcr.2017.04.11
4. Lee HY, Cha MJ, Lee KS, et al. Prognosis in resected invasive mucinous adenocarcinomas of the lung: related factors and comparison with resected nonmucinous adenocarcinomas. *J Thorac Oncol*. 2016;11(7):1064–1073. doi:10.1016/j.jtho.2016.03.011
5. Watanabe H, Saito H, Yokose T, et al. Relation between thin-section computed tomography and clinical findings of mucinous adenocarcinoma. *Ann Thorac Surg*. 2015;99(3):975–981. doi:10.1016/j.athoracsur.2014.10.065
6. Lee MA, Kang J, Lee H, et al. Spread through air spaces (STAS) in invasive mucinous adenocarcinoma of the lung: incidence, prognostic impact, and prediction based on clinicoradiologic factors. *Thorac Cancer*. 2020;11(11):3145–3154. doi:10.1111/1759-7714.13632
7. Cha YJ, Shim HS. Biology of invasive mucinous adenocarcinoma of the lung. *Transl Lung Cancer Res*. 2017;6(5):508–512. doi:10.21037/tlcr.2017.06.10
8. Shimizu K, Okita R, Saisho S, et al. Clinicopathological and immunohistochemical features of lung invasive mucinous adenocarcinoma based on computed tomography findings. *Onco Targets Ther*. 2016;28(10):153–163. doi:10.2147/OTT.S121059
9. Yin JC, Xi JJ, Liang JQ, et al. Solid components in the mediastinal window of computed tomography define a distinct subtype of subsolid nodules in clinical stage I lung cancers. *Clin Lung Cancer*. 2021;22(4):324–331. doi:10.1016/j.cllc.2021.02.015
10. Cha YJ, Kim HR, Lee HJ, et al. Clinical course of stage IV invasive mucinous adenocarcinoma of the lung. *Lung Cancer*. 2016;102:82–88. doi:10.1016/j.lungcan.2016.11.004
11. Wang Y, Liu J, Huang C, et al. Development and validation of a nomogram for predicting survival of pulmonary invasive mucinous adenocarcinoma based on Surveillance, Epidemiology, and End Results (SEER) database. *BMC Cancer*. 2021;21(1):148. doi:10.1186/s12885-021-07811-x
12. Guo M, Tomoshige K, Meister M, et al. Gene signature driving invasive mucinous adenocarcinoma of the lung. *EMBO Mol Med*. 2017;9(4):462–481. doi:10.15252/emmm.201606711
13. Miyamoto A, Kurosaki A, Fujii T, et al. HRCT features of surgically resected invasive mucinous adenocarcinoma associated with interstitial pneumonia. *Respirology*. 2017;22(4):735–743. doi:10.1111/resp.12947
14. Miyata N, Endo M, Nakajima T, et al. High-resolution computed tomography findings of early mucinous adenocarcinomas and their pathologic characteristics in 22 surgically resected cases. *Eur J Radiol*. 2015;84(5):993–997. doi:10.1016/j.ejrad.2015.01.014
15. Yang W, Sun Y, Fang W, et al. High-resolution computed tomography features distinguishing benign and malignant lesions manifesting as persistent solitary subsolid nodules. *Clin Lung Cancer*. 2018;19(1):e75–e83. doi:10.1016/j.cllc.2017.05.023
16. Cha MJ, Lee KS, Kim TJ, et al. Solitary nodular invasive mucinous adenocarcinoma of the lung: imaging diagnosis using the morphologic-metabolic dissociation sign. *Korean J Radiol*. 2019;20(3):513–521. doi:10.3348/kjr.2018.0409
17. Beck KS, Sung YE, Lee KY, et al. Invasive mucinous adenocarcinoma of the lung: serial CT findings, clinical features, and treatment and survival outcomes. *Thorac Cancer*. 2020;11(12):3463–3472. doi:10.1111/1759-7714.13674
18. Wang T, Yang Y, Liu X, et al. Primary invasive mucinous adenocarcinoma of the lung: prognosticValue of CT imaging features combined with clinical factors. *Korean J Radiol*. 2021;22(4):652–662. doi:10.3348/kjr.2020.0454
19. Kawaguchi Y, Nakao M, Omura K, et al. The utility of three-dimensional computed tomography for prediction of tumor invasiveness in clinical stage IA lung adenocarcinoma. *J Thorac Dis*. 2020;12(12):7218–7226. doi:10.21037/jtd-20-2131
20. Miao YY, Zhang JY, Zou JW, et al. Correlation in histological subtypes with high resolution computed tomography signatures of early stage lung adenocarcinoma. *Transl Lung Cancer Res*. 2017;6(1):14–22. doi:10.21037/tlcr